Ferromagnetism and the Formation of Interlayer As_2 Dimers in $Ca(Fe_{1-x}Ni_x)_2As_2$

Roman Pobel, Rainer Frankovsky and Dirk Johrendt

Department Chemie der Ludwig-Maximilians-Universität München, Butenandtstraße 5 – 13 (Haus D), 81377 München, Germany

Reprint requests to Prof. Dr. Dirk Johrendt. Fax: 089-2180 77431. E-mail: johrendt@lmu.de

Z. Naturforsch. **2013**, *68b*, 581 – 586 / DOI: 10.5560/ZNB.2013-3045
Received February 13, 2013

Dedicated to Professor Heinrich Nöth on the occasion of his 85th birthday

The compounds $Ca(Fe_{1-x}Ni_x)_2As_2$ with the tetragonal $ThCr_2Si_2$-type structure (space group $I4/mmm$) show a continuous transition of the interlayer As–As distances from a non-bonding state in $CaFe_2As_2$ ($d_{As-As} = 313$ pm) to single-bonded As_2 dimers in $CaNi_2As_2$ ($d_{As-As} = 260$ pm). Magnetic measurements have revealed weak ferromagnetism which develops near the composition $Ca(Fe_{0.5}Ni_{0.5})_2As_2$, while the compounds with lower and higher nickel concentrations are both Pauli-paramagnetic. DFT band structure calculations have shown that the As_2 dimer formation is a consequence of weaker metal-metal bonding in the $MAs_{4/4}$ layers ($M = Fe_{1-x}Ni_x$) of the Ni-rich compounds, and depends not on depopulation or shift of As–As σ^* antibonding states as previously suggested. Our results also show that the ferromagnetism of $Ca(Fe_{0.5}Ni_{0.5})_2As_2$ and related compounds like $SrCo_2(Ge_{0.5}P_{0.5})_2$ is not as recently suggested induced by dimer breaking, but arises from the high density of states generated by the transition metal 3*d* bands near the Fermi level without contribution from dimers.

Key words: Intermetallic Compounds, Crystal Structures, $ThCr_2Si_2$-type Structure, Chemical Bonding, Ferromagnetism

Introduction

The discovery of high-T_c superconductivity in iron arsenides has renewed the interest in transition metal pnictides [1 – 4], and especially compounds with the tetragonal $ThCr_2Si_2$-type structure like $BaFe_2As_2$ and its derivatives rank among the most intensively investigated materials [5 – 8]. Currently further structure-property relationships of the $ThCr_2Si_2$-type compounds also attract considerable attention, among them the remarkable flexibility of the homonuclear bond between the pnictide atoms of adjacent layers. The whole range from long non-bonding distances up to short single-bonded dimers, as well as structural phase transitions between both states have been observed [9 – 11]. Fig. 1 shows the structures of $CaFe_2As_2$ with pairs of isolated As^{3-} anions ($d_{As-As} = 313$ pm) [12], and $CaNi_2As_2$ with As_2^{4-} anions ($d_{As-As} = 260$ pm) [13]. It has long been known that the tendency to form these bonds increases within the 3*d* transition metal period from left to right. A continuous transition between these states has recently been described for solid solutions of the phosphides $Ca(Co_{1-x}Ni_x)_2P_2$ [14].

Atom size arguments are obviously ruled out in these cases, and thus an electronic origin of these remarkable bond length changes is expected. A widely accepted explanation had been suggested already in 1985 by Hoffmann and Zheng based on semi-empirical band structure calculations of Mn_2P_2 layers [15]. They argued that P–P σ^* antibonding orbitals become depopulated as the Fermi level of the metal decreases upon band filling along the 3*d* series. Subsequent calculations based on density functional theory (DFT) have not supported this concept [16, 17]. However, a better understanding of the electronic mechanism of interlayer bond formation is very important with respect to the physical properties of $ThCr_2Si_2$-type compounds. The transition from the non-bonded to the bonded state may significantly change the electronic

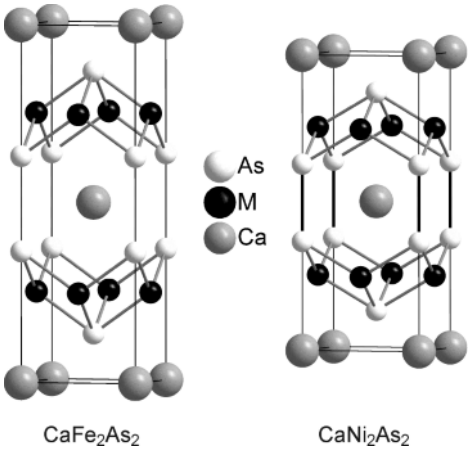

Fig. 1. Crystal structures of $CaFe_2As_2$ (M = Fe) and $CaNi_2As_2$ (M = Ni).

state at the transition metal atoms and also the Fermi surface, both crucial for electronic and magnetic properties. As an example, it is believed that the absence of superconductivity in $CaFe_2As_2$ under pressure [18], in contrast to $BaFe_2As_2$ and $SrFe_2As_2$ [19], has its origin in the formation of As_2 dimers in $CaFe_2As_2$ at pressures still too low to induce superconductivity, while $BaFe_2As_2$ keeps the structure with non-bonded As^{3-} under pressure. Further examples are magnetic transitions in EuM_2P_2 (M = Co, Fe) [20, 21], or the recent observation of ferromagnetism that develops during the course of breaking Ge_2 dimers in $SrCo_2(Ge_{1-x}P_x)_2$ [22].

In this article we report the synthesis, crystal structure and magnetism of the solid solutions $Ca(Fe_{1-x}Ni_x)_2As_2$ which show the gradual formation of As_2 dimers with increasing nickel concentration while weak ferromagnetism develops near $x \approx 0.5$. Concomitant changes of the electronic structure are studied by DFT band calculations together with bond analysis using the COHP method.

Results and Discussion

Crystal structure

Fig. 2 shows the lattice parameters of the solid solution $Ca(Fe_{1-x}Ni_x)_2As_2$. The c axis contracts strongly with x by about −20 %, while the a axis is slightly elongated by only 4 %. The changes are not linear but rather S-shaped with steeper slopes between $x = 0.3$ and $x = 0.5$. In Fig. 3 we compare the variations of the normalized bond lengths and the twofold angle As–M–As (ε). Most strikingly, the As–As distance between the layers becomes shortened by −20 %, thus the transition from the state with single As atoms in $CaFe_2As_2$ to an As_2 dimer in $CaNi_2As_2$ is evident. The enormous shortening is at the expense of increased M–M distances (+4 %), while the strong M–As bonds of the tetrahedra remain almost unaffected. In other words, the $MAs_{4/4}$ tetrahedron becomes flatter, which is manifested in the increasing As–M–As bond angle ε.

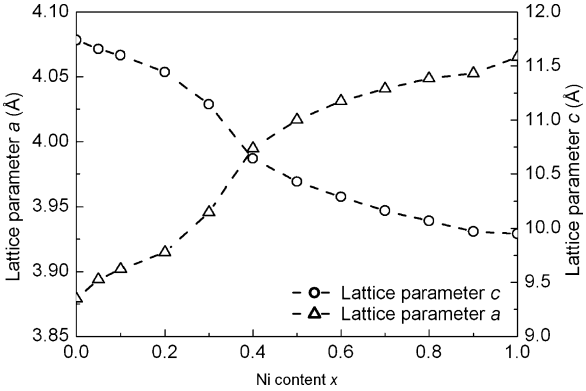

Fig. 2. Lattice parameters of the solid solution $Ca(Fe_{1-x}Ni_x)_2As_2$.

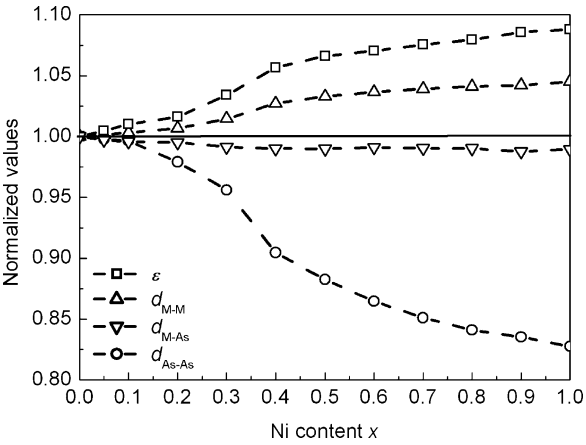

Fig. 3. Normalized changes of bond lengths and the As–M–As bond angle (ε) in $Ca(Fe_{1-x}Ni_x)_2As_2$.

Magnetic properties

The stripe-type antiferromagnetic order of $CaFe_2As_2$ (T_N = 173 K) has already been com-

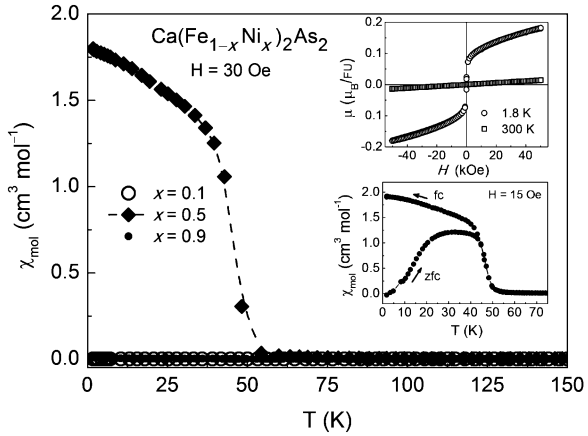

Fig. 4. Magnetic susceptibilities of $Ca(Fe_{1-x}Ni_x)_2As_2$ ($x = 0.1$, 0.5, 0.9) measured in a 30 Oe field. Upper inset: isothermal magnetizations of $Ca(Fe_{0.5}Ni_{0.5})_2As_2$ at 300 and 1.8 K; lower inset: low-temperature susceptibility of $Ca(Fe_{0.5}Ni_{0.5})_2As_2$ measured in zero-field-cooling (zfc) and field-cooling (fc) modes.

prehensively investigated [23]. Fig. 4 shows the results of magnetic measurements with samples of $Ca(Fe_{1-x}Ni_x)_2As_2$ at $x = 0.1$, 0.5 and 0.9. The small ($\approx 10^{-4}$ cm^3 mol^{-1} at 150 K) and weakly temperature-dependent susceptibilities of $Ca(Fe_{0.9}Ni_{0.1})_2As_2$ and $Ca(Fe_{0.1}Fe_{0.9})_2As_2$ are consistent with Pauli-paramagnetic behavior, while $Ca(Fe_{0.5}Ni_{0.5})_2As_2$ shows a sudden increase of χ_{mol} below 50 K which indicates ferromagnetic ordering. The magnetization isotherm at 300 K is linear, while at 1.8 K (inset of Fig. 4) the magnetization strives after saturation towards a weak moment of 0.2 μ_B per formula unit. Kink point measurements in field-cooled and zero-field-cooled modes (inset of Fig. 4) support the presence of ferromagnetism. The derivatives $d\chi/dT$ yielded Curie temperatures of 47 K (zfc) and 46 K (fc).

Electronic structure and chemical bonding

Fig. 5 shows the projected density of states (PDOS) of the transition metals *M* (solid lines), and the As contributions (filled areas) in $CaFe_2As_2$, $CaFeNiAs_2$ and $CaNi_2As_2$, together with plots of the integrated COHP (ICOHP) of *M*–As, As–As, and *M*–*M* bonds. ICOHP measures the energy contributions of the specified bonds to the total band structure energy. The PDOS plots of all three compounds are remarkably similar despite significant changes in the bond lengths

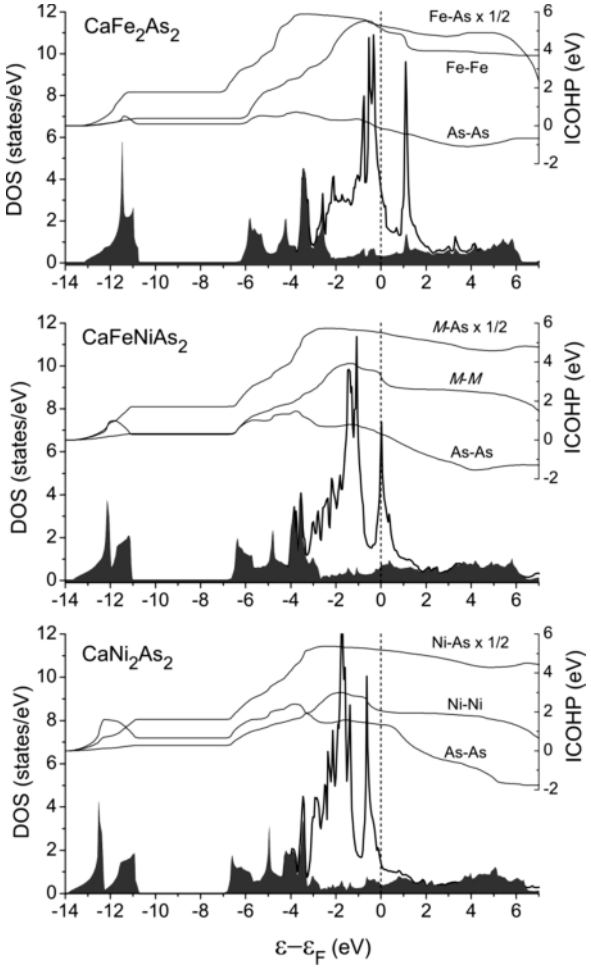

Fig. 5. Partial density of states (PDOS) of the metal 3*d* (lines) and arsenic 4*s*/*p* contributions (filled areas), together with the ICOHP curves of the *M*–As, *M*–*M* and As–As bonds, respectively.

and in the valence electron count (VEC), which increases from 28 in $CaFe_2As_2$ to 32 in $CaNi_2As_2$. The Fermi level (dashed vertical line) traverses a sharp peak in the PDOS of the metal and coincides with it in the case of $CaFeNiAs_2$ (VEC = 30). The origin of this peak is the *M*–*M* antibonding band of $dd\sigma^*$ symmetry. Also remarkable are the similar distributions of the As PDOS in spite of the large variation of the As–As distances from 313 to 260 pm. In all cases, the As 4*p* orbital energies spread from −6 to +6 eV, while the As 4*s* orbital energies are between −13 and −11 eV. In contrast to the Hoffmann model [15] we find no significant change of the As band filling in spite of the in-

creased VEC. Fig. 5 also shows only a small contribution of the As bands to the density of states at the Fermi level, which is dominated by the metal 3*d* orbitals. Starting from $CaFe_2As_2$, the additional electrons populate mainly 3*d* bands, and scarcely As *p* bands. Thus it becomes clear that the observed changes of the crystal structure and physical properties indeed originate from 3*d* band filling, but not from depopulation of As–As σ^* antibonding orbitals.

The ICOHP plots in Fig. 5 reflect the strengths of the bonding interactions. The *M*–As bonds are by far the strongest ($\sim$ 10 eV per cell) and remain almost unaffected by the VEC. Remarkably, the Fe–Fe bonds in $CaFe_2As_2$ (VEC = 28) are the second strongest (4.5 eV per cell), while the As–As bonding contribution is almost zero. When the VEC increases to 30 in $CaFeNiAs_2$, the *M*–*M* bonds become significantly weaker (3 eV per cell, −33 %). We point out, that this is only partially caused by filling of the antibonding states near E_F, because the *M*–*M* ICOHP is inherently much smaller than in the case of iron as a result of the weaker overlap of the contracted Ni 3*d* orbitals. The As–As bond energy is still very small and negligible at the As–As distance of 280 pm in $CaFeNiAs_2$. These trends continue in $CaNi_2As_2$, where the Ni–Ni bond energy is reduced to 2 eV per cell, which is 50 % less than in the iron compound. The As–As distance is only 260 pm, and the corresponding bond energy contribution becomes significant. However, the overall energy contribution is only $\sim$ 1 eV per cell. The Fermi energy lies between As–As bonding and antibonding states in all three compounds, and it is the bonding character of these bands that changes rather than the band occupation. The changes in the ICOHP bond energies with the valence electron count are compiled in Fig. 6. Note that the metal-metal bonds still dominate over the As–As bonds even in $CaNi_2As_2$ with VEC = 32.

Our analysis reveals that the increasing electron count mainly affects the metal-metal bonds. Higher VEC leads to weaker *M*–*M* bonds, which causes longer *a*, *b* lattice parameters and flatter MAs_4 tetrahedra. As a result, the interlayer distance becomes smaller, and interlayer bonds can be formed. Thus the formation of the As_2 dimers is not caused by a depopulation of As–As σ^* orbitals as previously thought, but a consequence of the weakened *M*–*M* bonding in the $MAs_{4/4}$ layer.

The magnetism observed in the solid solutions $Ca(Fe_{1-x}Ni_x)_2As_2$ close to $x = 0.5$ is also understandable from the electronic structure. When the VEC is around 30 ($CaFeNiAs_2$), the Fermi energy coincides with the peak in the DOS (Fig. 5), and the Stoner criterion that favors a magnetic ground state is fulfilled. Magnetic ordering in $CaCo_2As_2$ [24] and $CaCo_2P_2$ [25] supports this argument. We also believe that the recently reported weak ferromagnetism in $SrCo_2(Ge_{0.5}P_{0.5})_2$ (VEC = 29) is caused by this DOS peak in the Co 3*d* states, and not by the intermediate *X*–*X* (*X* = Ge, P) bonding state as suggested in ref. [22].

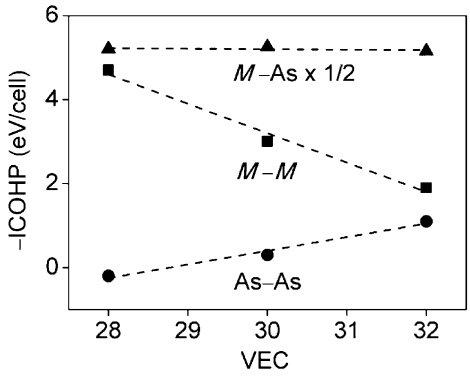

Fig. 6. Plot of the calculated ICOHP bond energies *vs.* the valence electron count (*M* = Fe, Ni).

Conclusion

The structures of the solid solutions $Ca(Fe_{1-x}Ni_x)_2As_2$ show the transition between the $ThCr_2Si_2$ type without As–As bonds between the layers (better referred to as the $BaZn_2P_2$ type [26, 27]) and the true $ThCr_2Si_2$-type structure with As_2 dimers. Our results indicate that the role of the homonuclear bonds between the layers of the $ThCr_2Si_2$-type structure is rather overrated. The As 4*p* orbitals spread over a large energy range, therefore any shifts of the Fermi level hardly affect their occupation. Thus the earlier interpretation of "making and breaking bonds" in the $ThCr_2Si_2$-type compounds does not correspond to the real situation. The electronic states at the Fermi level are clearly dominated by the transition metal 3*d* band, in particular a large peak in the DOS coincides with the Fermi energy when the band filling is close to 30 electrons per formula unit. Even though this peak is antibonding with respect to the metal-metal bonds in the layers, the ICOHP analysis shows that its occupation has no strong effect in weakening the

metal-metal bonds. Nevertheless it turned out that the metal-metal bonds inside the layers are the by far most affected. For the occupied states the *M–M* bonding character strongly decreases while going from iron to nickel, because the proceeding contraction of the 3*d* orbitals reduces the overlap and weakens the *M–M* bonds. We note that 3*d* orbital contraction had also been one argument of the Hoffmann model, but in the sense that this lowers the Fermi level and depopulates P–P σ^* orbitals, which is ruled out by our first-principle calculations.

Also the occurrence of the magnetic groundstate of $ThCr_2Si_2$-type compounds with 3*d* transition metals and nearly 30 valence electrons is not correlated to anion dimer "making or breaking" as suggested in a recent study [22]. Weak ferromagnetism develops near $x \approx 0.5$ in the solid solutions $Ca(Fe_{1-x}Ni_x)_2As_2$, where the VEC is close to 30. This magnetism is a consequence of a DOS peak from flat 3*d* bands, which coincides with the Fermi level at 30 electrons per unit cell. In this case the Stoner criterion is fulfilled, and ferromagnetism can emerge without significant contributions of the pnictide orbitals.

Experimental Section

Synthesis and powder X-ray diffraction

Polycrystalline samples were synthesized in alumina crucibles by mixing stoichiometric amounts of Ca (99.99 %), Fe (99.9 %), Ni (99.99 %), and As (99.999 %) in a glove box with purified argon atmosphere. The crucibles were subsequently sealed in silica tubes under argon atmosphere. The reaction mixtures were then heated to 773 K for 10 h, to 1033 K for 15 h and to 1273 K for 15 h before cooling to room temperature at a rate of $100\,K\,h^{-1}$. This first reaction step was followed by two annealing steps at 1173 K of which the second one was performed after pressing the homogenized sample into a pellet. The samples were characterized using powder X-ray diffraction with Cu $K_{\alpha 1}$ or Co $K_{\alpha 1}$ radiation. (Huber G670 Guinier imaging plate diffractometer). Rietveld refinements were performed using the TOPAS program package [28].

Magnetic measurements

Magnetic susceptibility measurements were performed on a Quantum Design MPMS XL5 SQUID magnetometer which allowed for measurements with fields between −50 and 50 kOe at temperatures between 1.8 and 400 K ($1\,kOe = 7.96 \times 10^4\,A\,m^{-1}$).

Electronic structure calculations

Self-consistent DFT band structure calculations were performed using the LMTO method in its scalar-relativistic version (program TB-LMTO-ASA) [29–31]. Reciprocal space integrations were performed with the tetrahedron method using 3013 irreducible *k* points in the tetragonal Brillouin zone. The basis sets were Ca-4*s*/[4*p*]/3*d*, Fe(Ni)-4*s*/4*p*/3*d* and As-4*s*/4*p*/[4*d*]. Orbitals in brackets were downfolded. The COHP (Crystal orbital Hamilton population) [32, 33] method was used for the bond analysis. COHP gives the energy contributions of all electronic states for a selected bond. The values are negative for bonding and positive for antibonding interactions. With respect to the widely used COOP diagrams, we plot negative COHP(*E*) to get positive values for bonding states.

Acknowledgement

This work has been supported financially by the German Research Foundation DFG within priority program SPP1458 under grant JO257/6.

[1] Y. Kamihara, T. Watanabe, M. Hirano, H. Hosono, *J. Am. Chem. Soc.* **2008**, *130*, 3296.
[2] D. Johrendt, R. Pöttgen, *Angew. Chem. Int. Ed.* **2008**, *47*, 4782.
[3] D. Johrendt, H. Hosono, R. D. Hoffmann, R. Pöttgen, *Z. Kristallogr.* **2011**, *226*, 435.
[4] D. Johrendt, *J. Mater. Chem.* **2011**, *21*, 13726.
[5] M. Pfisterer, G. Nagorsen, *Z. Naturforsch.* **1980**, *35b*, 703.
[6] M. Pfisterer, G. Nagorsen, *Z. Naturforsch.* **1983**, *38b*, 811.
[7] M. Rotter, M. Tegel, I. Schellenberg, W. Hermes, R. Pöttgen, D. Johrendt, *Phys. Rev. B* **2008**, *78*, 020503(R).
[8] M. Rotter, M. Pangerl, M. Tegel, D. Johrendt, *Angew. Chem. Int. Ed.* **2008**, *47*, 7949.
[9] C. Huhnt, G. Michels, M. Roepke, W. Schlabitz, A. Wurth, D. Johrendt, A. Mewis, *Physica B* **1997**, *240*, 26.
[10] A. Wurth, D. Johrendt, A. Mewis, C. Huhnt, G. Michels, M. Roepke, W. Schlabitz, *Z. Anorg. Allg. Chem.* **1997**, *623*, 1418.
[11] V. Keimes, D. Johrendt, A. Mewis, C. Huhnt, W. Schlabitz, *Z. Anorg. Allg. Chem.* **1997**, *623*, 1699.
[12] G. Wu, H. Chen, T. Wu, Y. L. Xie, Y. J. Yan, R. H. Liu, X. F. Wang, J. J. Ying, X. H. Chen, *J. Phys.: Condens. Matter* **2008**, *20*, 422201.

[13] A. Mewis, A. Distler, *Z. Naturforsch.* **1980**, *35b*, 391.
[14] S. A. Jia, S. X. Chi, J. W. Lynn, R. J. Cava, *Phys. Rev. B* **2010**, *81*, 214446.
[15] R. Hoffmann, C. Zheng, *J. Phys. Chem.* **1985**, *89*, 4175.
[16] E. Gustenau, P. Herzig, A. Neckel, *J. Solid State Chem.* **1997**, *129*, 147.
[17] D. Johrendt, C. Felser, O. Jepsen, O. K. Andersen, A. Mewis, J. Rouxel, *J. Solid State Chem.* **1997**, *130*, 254.
[18] W. Yu, A. A. Aczel, T. J. Williams, S. L. Bud'ko, N. Ni, P. C. Canfield, G. M. Luke, *Phys. Rev. B* **2009**, *79*, 020511.
[19] P. L. Alireza, Y. T. C. Ko, J. Gillett, C. M. Petrone, J. M. Cole, G. G. Lonzarich, S. E. Sebastian, *J. Phys.: Condens. Matter* **2009**, *21*, 012208.
[20] M. Chefki, M. M. Abd-Elmeguid, H. Micklitz, C. Huhnt, W. Schlabitz, M. Reehuis, W. Jeitschko, *Phys. Rev. Lett.* **1998**, *80*, 802.
[21] B. Ni, M. M. Abd-Elmeguid, H. Micklitz, J. P. Sanchez, P. Vulliet, D. Johrendt, *Phys. Rev. B* **2001**, *63*, 100102/1.
[22] S. A. Jia, P. Jiramongkolchai, M. R. Suchomel, B. H. Toby, J. G. Checkelsky, N. P. Ong, R. J. Cava, *Nature Phys.* **2011**, *7*, 207.
[23] A. I. Goldman, D. N. Argyriou, B. Ouladdiaf, T. Chatterji, A. Kreyssig, S. Nandi, N. Ni, S. L. Bud'ko, P. C. Canfield, R. J. McQueeney, *Phys. Rev. B* **2008**, *78*, 100506.
[24] B. Cheng, B. F. Hu, R. H. Yuan, T. Dong, A. F. Fang, Z. G. Chen, G. Xu, Y. G. Shi, P. Zheng, J. L. Luo, N. L. Wang, *Phys. Rev. B* **2012**, *85*, 144426.
[25] M. Reehuis, W. Jeitschko, G. Kotzyba, B. I. Zimmer, X. Hu, *J. Alloys Compd.* **1998**, *266*, 54.
[26] P. Klüfers, A. Mewis, *Z. Naturforsch.* **1978**, *33b*, 151.
[27] D. Schmitz, W. Bronger, *Z. Anorg. Allg. Chem.* **1987**, *553*, 248.
[28] A. Coelho, TOPAS Academic, Coelho Software, Brisbane (Australia) **2007**.
[29] H. L. Skriver, *The LMTO method – muffin tin orbitals and electronic structure*, Springer Verlag, Berlin, **1984**.
[30] O. K. Andersen, O. Jepsen, M. Sob, in *Electronic Band Structure and its Applications*, Lecture Notes in Physics, Vol. 283 (Ed.: M. Yussouff), Springer Verlag, Berlin, **1987**, pp. 1.
[31] O. K. Andersen, O. Jepsen, Tight-Binding LMTO, Max-Planck-Institut für Festkörperforschung, Stuttgart (Germany) **1994**.
[32] R. Dronskowski, P. E. Blöchl, *J. Phys. Chem.* **1993**, *97*, 8617.
[33] F. Boucher, R. Rousseau, *Inorg. Chem.* **1998**, *37*, 2351.